HHS Public Access

Author manuscript

Nature. Author manuscript; available in PMC 2009 November 07.

Published in final edited form as:

Nature. 2009 May 7; 459(7243): 93–97. doi:10.1038/nature07860.

Calcium/synaptotagmin-evoked compound fusion increases quantal size and synaptic strength

Liming He[1,*], **Lei Xue**[1,*], **Jianhua Xu**[1], **Benjamin D. McNeil**[1], **Li Bai**[1], **Ernestina Melicoff**[2], **Roberto Adachi**[2], and **Ling-Gang Wu**[1]

[1]National Institute of Neurological Disorders and Stroke, 35 Convent Dr., Bldg 35, Rm. 2B-1012, Bethesda, Maryland 20892

[2]Department of Pulmonary Medicine, The University of Texas M. D. Anderson Cancer Center, 2121 W. Holcombe Blvd., Box 1100, Houston, Texas 77030

Abstract

Exocytosis at synapses generally refers to fusion between vesicles and the plasma membrane1. Although compound fusion between vesicles2,3 was proposed at ribbon-type synapses4,5, whether it exists, how it is mediated, and what role it plays at conventional synapses remain unclear. Here we addressed this issue at a nerve terminal containing conventional active zones. High potassium application and high frequency firing induced giant capacitance up-steps reflecting exocytosis of vesicles larger than regular ones, followed by giant down-steps reflecting bulk endocytosis. They also induced giant vesicle-like structures, as observed with electron microscopy, and giant miniature EPSCs (mEPSCs) reflecting more transmitter release. Calcium and its sensor for vesicle fusion, synaptotagmin, were required for these giant events. After high frequency firing, calcium/synaptotagmin-dependent mEPSC size increase was paralleled by calcium/synaptotagmin-dependent post-tetanic potentiation (PTP). These results suggest that calcium/synaptotagmin mediates compound fusion between vesicles, that exocytosis of compound vesicles increases quantal size which enhances synaptic strength and thus contributes to the generation of PTP, and that exocytosed compound vesicles may be retrieved via bulk endocytosis. We suggest to include a new vesicle cycling route, compound exocytosis followed by bulk endocytosis, into models of synapses, where currently only vesicle fusion with the plasma membrane is considered (Fig. S1)1.

We performed cell-attached capacitance recordings at the release face of calyces (Fig. 1a)6. Unless mentioned, rats were used. Before KCl application (control), spontaneous up-steps occurred at 0.008 ± 0.001 Hz (n = 78 patches, Fig. 1a, see Methods). About 94% of up-steps were < 220 aF (mean = 84 ± 4 aF, n = 96 up-steps). The remaining 6% were 220 – 380 aF (mean = 275 ± 22 aF, n = 6 up-steps, Fig. 1b). A regular vesicle's capacitance is ∼23 – 220 aF, because the vesicle diameter is ∼30 – 80 nm in calyces7, and the specific membrane

---

Correspondence to: Ling-Gang Wu.

*equal contribution

capacitance is 8 – 11 fF/μm^2 (Ref. 8). Thus, most up-steps in control were caused by single vesicle fusion (see also Ref. 6).

KCl application (∼50 – 100 mM, unless mentioned) increased the up-step frequency to 0.16 ± 0.02 Hz (n = 17 patches, Fig. 1a, see Methods). The up-step amplitude distribution and cumulative probability curve were shifted to the right, compared to control (Fig. 1b, Kolmogorov-Smirnov test, $p < 0.001$). The mean of all up-steps was 193 ± 9 aF (n = 857), or ∼203% of control (95 ± 5 aF, n = 102, $p < 0.01$). About 20% of up-steps were > 220 aF, a regular vesicle's maximal capacitance (Fig. 1a, b), and were called 'giant' up-steps. Their mean was 571 ± 37 aF (n = 174 up-steps) and the largest was 2878 aF, or 34 – 40 times the mean of regular vesicles (73 aF in Ref. 6, 84 aF here). Both the percentage and the mean size of giant up-steps were significantly higher than control (χ^2 test & t test, $p < 0.01$). Even when up-steps between 100 – 220 aF were measured, KCl significantly increased the amplitude from 133 ± 6 aF (n = 28) in control to 144 ± 2 aF (n = 294, $p < 0.05$), suggesting compound fusion between 2 – 3 regular vesicles. Thus, up-step size increase was not limited to giant up-steps.

Giant up-steps were not caused by dense-core vesicle fusion, as dense-core vesicles are rare in calyces7. Giant up-steps were not composed of multiple small up-steps, because, even when the time resolution was increased to 0.6 – 0.9 ms, giant up-steps rose from 20 – 80% in one step (n = 44 giant up-steps, 3 patches, Fig. 1a). In 6% of giant up-steps, we detected an initial fusion pore conductance (G_p) of 162 ± 41 pS (n = 10 up-steps), which gradually increased for ∼10 – 230 ms, and ended in rapid pore expansion (Fig. 1c). G_p in remaining giant up-steps was too large or fast to resolve (Fig. 1a). Most giant up-steps could not be explained by independent fusion of multiple vesicles, because the up-step frequency (∼0.16 Hz) was too low to account for the observed large percentage (∼20%) of giant up-steps (Supplementary Information II–1). Thus, giant up-steps reflect fusion of a single structure larger than regular vesicles.

KCl application also increased the frequency of down-steps, which reflected endocytosis, from 0.006 ± 0.002 Hz in control (n = 78 patches) to 0.10 ± 0.01 Hz (n = 17 patches; $p < 0.01$, Fig. 1d), and shifted the down-step size distribution (Supplementary Information II–2) and cumulative probability curve to the right (Fig. 1e, Kolmogorov-Smirnov test, $p < 0.01$). The percentage (17%) and the mean amplitude (501 ± 42 aF, n = 102 down-steps; range: 220 – 2943 aF) of giant down-steps during KCl application were significantly higher than control (8%, χ^2 test, $p < 0.01$; 331 ± 31 aF, n = 6, $p < 0.01$). In 5% giant down-steps, we detected an initial fission pore conductance of 376 ± 113 pS (n = 5), corresponding to a pore with a diameter of 2.7 ± 1.5 nm, which reduced at 36 ± 11 pS/ms or 0.82 ± 0.46 nm/ms to an undetectable level (Fig. 1c). Thus, KCl induced more and larger giant down-steps, which reflect bulk endocytosis9–11.

Endosome-like structures formed by bulk endocytosis may undergo exocytosis12. For two reasons, this mechanism did not underlie giant up-steps. First, the first giant up-step occurred ∼80 s earlier than the first giant down-step after KCl application (n = 17 patches, $p < 0.001$, Fig. 1f, g), and was no later than the first regular-sized down-step (Supplementary Information II–3), suggesting that it was not caused by re-exocytosis of endocytic structures.

Second, when calyces were whole-cell dialyzed with GDPβS (0.3 mM) to block endocytosis13, the up-step frequency (0.24 ± 0.07 Hz, n = 6 patches) and the percentage (28%) of giant up-steps were similar to those without GDPβS ($p > 0.08$, e.g., Fig. 1h), indicating that giant up-steps were not caused by re-exocytosis of endocytic structures. GDPβS indeed blocked endocytosis, because only 1 down-step was observed within 300 s of KCl application in 6 cell-attached patches showing up-steps (Fig. 1h); whereas without GDPβS dialysis, down-steps were observed in all 17 patches showing up-steps (χ^2 test, $p < 0.01$).

Similar to KCl application, action potential trains at 100 Hz for 10 – 20 s, as induced by current injection with another cell-attached electrode at the calyx (Fig. 2a, n = 5)14, increased the up-step frequency from 0.011 ± 0.011 Hz (before stimulation) to 0.465 ± 0.078 Hz during stimulation (n = 6, $p < 0.01$) and to 0.040 ± 0.018 Hz within 50 s after stimulation. Action potential trains induced a large number of giant up-steps (9 out of 56 up-steps during, 5 out of 11 up-steps after, Fig. 2a).

Calcium binding with synaptotagmin II (Syt2) mediates evoked release at calyces14. Two pieces of evidence suggest that calcium/Syt2 mediates giant up-steps. First, after removing the extracellular calcium, giant up-steps were observed in 1 out of 21 patches during KCl application (Fig. 2b), which was significantly lower than control (17 out of 55 patches, χ^2 test, $p < 0.01$). Thus, like regular up-steps6, calcium influx induced giant up-steps. Second, similar to results obtained in rats, in *Syt2*$^{+/+}$ mice, KCl increased the up-step frequency from 0.003 ± 0.001 Hz to 0.14 ± 0.02 Hz (n = 11 patches, $p < 0.001$), the amplitude from 79 ± 16 aF (n = 26) to 216 ± 9 aF (n = 483, $p < 0.01$), and the giant up-step percentage to 24% (Fig. 2c, d). Compared to these results, *Syt2*$^{-/-}$ calyces showed a higher up-step frequency at rest (0.13 ± 0.04 Hz, n = 10 patches, $p < 0.01$) with a similar amplitude (80 ± 5 aF, n = 220, $p > 0.9$, Fig. 2e, f). Only 5% of up-steps were >220 aF in *Syt2*$^{-/-}$ mice at rest, similar to results obtained in rats. In *Syt2*$^{-/-}$ mice, KCl application slightly increased the up-step frequency to 0.25 ± 0.08 Hz (n = 10 patches, $p < 0.05$) without increasing the mean up-step amplitude (87 ± 3 aF, n = 834, $p > 0.2$; Fig. 2e, f) or the giant up-step percentage (3.8%, χ^2 test, $p = 0.26$). Thus, Syt2 mediated most KCl-induced up-steps, including giant ones.

If calcium/Syt2-mediated giant up-steps reflect exocytosis of compound vesicles produced by compound fusion between vesicles2,3, KCl must induce Syt2-dependent giant vesicles and mEPSCs. These predictions were tested below. First, at 1 min after KCl application, a time when giant down-steps reflecting bulk endcytosis rarely occurred (Fig. 1f, g), electron microscopy (EM) revealed that the vesicle diameter increased from 47.2 ± 0.4 nm (n = 2896 vesicles) in control to 57.8 ± 0.9 nm (n = 2040 vesicles from 6 rats, $p < 0.001$, Fig. 2g, h). About 13% of vesicles had a diameter from 80 to > 300 nm. These giant vesicles may have a membrane capacitance of ∼220 aF to > 2550 aF (Ref. 8), agreeing with the giant up-step amplitude range (220 – 2878 aF, Fig. 1b). Similar results were observed at 1.5 – 2 min after KCl application in 4 rats and 4 *Syt2*$^{+/+}$ mice. Our observation of large organelles (see also Ref. 10) made the occurrence of compound fusion physically possible. In *Syt2*$^{-/-}$ mice, however, 1.5 min KCl application did not increase the vesicle diameter, supporting that Syt2 mediates compound fusion (control: 46.3 ± 0.3 nm, n = 1298 vesicles, 4 mice; KCl: 47 ± 0.5 nm, n = 1053 vesicles, 4 mice, $p > 0.3$, Fig. 2i, j).

Second, KCl application for 2 – 3 min increased the mEPSC frequency from 0.72 ± 0.18 Hz to 6.37 ± 0.6 Hz (n = 21 neurons, $p < 0.01$), and the amplitude from 29.6 ± 1.0 pA to 44.9 ± 2.3 pA (n = 21, $p < 0.01$, Fig. 3a, b). The fraction of mEPSCs larger than a value between 50 – 200 pA was higher during KCl application than in control (n = 21 neurons, $p < 0.01$, Fig. 3b). The 10 – 90% rise time of mEPSCs > 80 pA (0.35 ± 0.01 ms) was slower than that for mEPSCs < 80 pA (0.29 ± 0.01 ms, n = 10 neurons, $p < 0.01$, Fig. 3c), consistent with simulation showing that larger vesicles generate larger and slower mEPSCs (Supplementary Information III–1). The mEPSC amplitude increase was due to a larger amount of released glutamate (Supplementary Information III–2), consistent with exocytosis of giant vesicles. AMPA receptor saturation by higher glutamate concentrations might explain why KCl increased the mEPSC amplitude by only ∼52%, but increased the up-step size by ∼103% (Supplementary Information III–3).

Two pieces of evidence indicated that calcium/Syt2 was required for KCl-induced increases of the mEPSC frequency and amplitude. First, removing extracellular calcium abolished KCl-induced increase of the mEPSC frequency and amplitude (n = 5 cells, Fig. 3d). Second, in $Syt2^{+/+}$ mice (n = 4), KCl significantly increased the mEPSC frequency (Ctrl: 0.7 ± 0.3 Hz; KCl: 7.8 ± 0.7 Hz, n = 6 synapses, $p < 0.01$, Fig. 3e) and amplitude (Ctrl: 31.8 ± 1.4 pA; KCl: 46.6 ± 3.7 pA, n = 6, $p < 0.01$, Fig. 3f), whereas in $Syt2^{-/-}$ mice (n = 6), KCl only slightly increased the mEPSC frequency (Ctrl: 13.9 ± 3.1 Hz; KCl: 18.8 ± 2.9 Hz, n = 9, $p < 0.01$, Fig. 3g), but not the mEPSC amplitude (Ctrl: 34.6 ± 1.1 pA; KCl: 35.3 ± 0.9 pA, n = 9, $p > 0.3$, Fig. 3h).

Giant up-steps after action potential trains (Fig. 2a) predicted giant mEPSCs. Indeed, action potential trains at 100 Hz for 4, 10 or 30 s increased the mEPSC amplitude, and induced post-tetanic potentiation (PTP) of the EPSC15,16 (Fig. 4a, b). Longer trains induced larger increases (Fig. 4a, b). The PTP decay was fitted with a bi-exponential function, whereas the mEPSC amplitude potentiation decayed approximately mono-exponentially (Fig. 4a). The amplitude and the time constant of the mEPSC amplitude potentiation matched the PTP slow component (Fig. 4b, $p > 0.3$), suggesting a causal relation between them. The mEPSC size increase was small after 4 s stimulation (10 ± 3%, n = 5, Fig. 4a), consistent with reports of negligible mEPSC size change15,16. Although these results were obtained in p6 – 10 rats, similar results were obtained in p13 – 14 rats (n = 3).

Bath application of the calcium buffer EGTA-AM (200 μM, ∼20 min) reduced the EPSC amplitude15,16 and abolished both the PTP15–17 and the mEPSC size increase induced by a 30 s train (n = 4, Fig. 4c). Deletion of Syt2 in mice decreased the EPSC14, and abolished both PTP and the mEPSC amplitude potentiation (Fig. 4d, e). Syt2 deletion also reduced the mEPSC frequency increase, as measured in the first minute after stimulation (2.8 ± 0.5 times from 7 synapses in $Syt2^{-/-}$ mice, but 11.5 ±0.5 times from 7 synapses in $Syt2^{+/+}$ littermates, $p < 0.01$), suggesting the involvement of Syt2 in the mEPSC frequency increase. Taken together, our results suggest that calcium/Syt2 mediates the mEPSC size increase, which generates the PTP slow component.

In summary, KCl application induced calcium/Syt2-dependent increases of up-steps (see also Supplementary Information IV), vesicle size, and the mEPSC amplitude and rise time,

suggesting that calcium/Syt2 mediates compound fusion, which forms compound vesicles. Subsequent exocytosis of compound vesicles increased the quantal size, which contributed to the generation of PTP. These results suggest to include compound fusion, along with vesicle fusion with the plasma membrane1, into the current model of exocytosis at synapses (Fig. S1).

Giant miniature currents or potentials (minis) observed at many synapses18–21 are inconsistent with quantal hypothesis, which assumes a single quantum for a mini22. Accordingly, multi-vesicular release was proposed18–21. Our results suggest that giant minis are caused by compound fusion and subsequent compound exocytosis. Consistent with this suggestion, giant organelles are present at synapses displaying giant minis18,19.

Multi-vesicular release was observed during stimulation at many synapses23–26. An alternative explanation to multi-vesicular release, compound fusion, was proposed4, and supported by a study revealing large organelles soon after ∼20 s stimulation at ribbon-type synapses, although bulk endocytosis as the cause of these large organelles was not fully excluded5. The present work suggests that compound fusion is an alternative explanation to multi-vesicular release at conventional synapses.

Large endosome-like structures were previously attributed to endocytosis9–12,27. They can now be reinterpreted at least partly as compound fusion (see also Ref. 5). We found that giant down-steps reflecting bulk endocytosis occurred later than giant up-steps, and correlated with giant up-steps in frequency and size (Supplementary Information V). We suggest that bulk endocytosis retrieves exocytosed compound vesicles via a mechanism that maintains the identity or at least the area of compound vesicles (Fig. S1).

PTP, which may control the neuronal circuit function17, was not considered to be caused by the quantal size increase, likely because at its peak, the mEPSC size increase was insufficient to account for PTP (Fig. 4a). The present work suggests that compound fusion-induced quantal size increase contributes to the generation of PTP. Compound fusion is likely a common mechanism used to enhance synaptic strength, because 1) PTP is observed at many synapses15,17; 2) intense firing that may generate PTP occurs in physiological and pathological conditions17,28,29; and 3) large organelles9–12,27 and giant mEPSCs18–21 that may be caused by compound fusion are widely observed.

Although compound fusion was found in non-neuronal secretory cells decades ago2,3, its underlying mechanism is unclear. The present work suggests that calcium binding with synaptotagmin mediates compound fusion, likely via interaction between v- and t-SNARE fusion proteins on the vesicle membrane30. The affinity of Syt2 for calcium is at tens of micromolar14. The transient calcium microdomain (tens of micromolar) induced by an action potential at the release site might expand greatly during prolonged stimulation, allowing for Syt2 to mediate fusion between vesicles beyond the plasma membrane. Consistent with this possibility, EGTA blocked the mEPSC size increase (Fig. 4c) likely by limiting the expansion of the calcium microdomain during high frequency stimulation.

Methods summary

For most experiments, parasagittal brainstem slices (200 μm thick) containing the medial nucleus of the trapezoid body were prepared from Wistar rats or mice (*Syt2*$^{-/-}$ or *Syt2*$^{+/+}$ littermates) using a vibratome6. Only for PTP experiments, horizontal brainstem slices were prepared, where a 0.1 ms, 2 – 20 V voltage pulse was applied via a bipolar electrode at the midline of the trapezoid body to evoke action potentials at the axon and calyx. If not mentioned, animals were 6 – 10 days old. We removed the postsynaptic neuron and performed cell-attached recordings of the imaginary (Im, capacitance) and the real (Re, conductance) components of the complex admittance at the release face of the calyces of Held6. Except Fig. 1a (right), Im and Re traces in all figures are low-pass filtered at 50 Hz. For traces in Fig. 1a (right), the low-pass filter in the lock-in amplifier was set at 0.1 ms. Means are presented as ± s.e.m. Unless mentioned, statistical test was t test. Detailed methods are described mostly in an online Methods section, and partly in Supplementary Information VI.

Methods

1. Bath and pipette solutions

For preparing slices, we used a solution containing (in mM): 95 NaCl, 25 $NaHCO_3$, 25 glucose, 50 sucrose, 2.5 KCl, 1.25 NaH_2PO_4, 0.1 $CaCl_2$, and 3 $MgCl_2$, 0.4 ascorbic acid, 3 *myo*-inositol, 2 sodium pyruvate (95% O_2/5% CO_2). Slices were incubated for 30 min at 37°C and then held at room temperature (22 – 24 ºC) for experiments in a solution containing (in mM): 125 NaCl, 2.5 KCl, 1 $MgCl_2$, 2 $CaCl_2$, 25 dextrose, 1.25 NaH_2PO_4, 0.4 ascorbic acid, 3 *myo*-inositol, 2 sodium pyruvate, 25 $NaHCO_3$, 0.001 TTX (preventing action potentials), pH 7.4 when bubbled with 95% O_2, 5% CO_2. When KCl concentration was increased (to 50 – 100 mM, if not mentioned), NaCl concentration was decreased to maintain the same osmolarity.

For cell-attached recordings and current injection (Fig. 1 – Fig. 2), the pipette (4 – 6 MΩ) contained (in mM): 130 NaCl, 2.5 KCl, 2 $CaCl_2$, 1 $MgCl_2$, 10 HEPES, 20 TEA, pH 7.2, adjusted with NaOH (osmolarity was 310 – 320 milliOsm).

For whole-cell dialysis of GDPβS (Fig. 1h), the pipette contained (in mM): 125 K-gluconate, 20 KCl, 10 Na_2-phosphocreatine, 4 MgATP, 0.3 GDPβS, 10 HEPES, 0.05 BAPTA, pH 7.2, adjusted with KOH. The calyx was under the current-clamp mode (EPC-10 amplifier, HEKA electronics, Lambrecht, Germany) while high potassium was applied to induce exocytosis.

For recordings of the postsynaptic AMPA receptor-mediated EPSC and mEPSC (Fig. 3 – Fig. 4), the pipette (2 – 3 MΩ) contained (in mM): 125 K-gluconate, 20 KCl, 4 MgATP, 10 Na_2-phosphocreatine, 0.3 GTP, 10 HEPES, and 0.5 EGTA, pH 7.2, adjusted with KOH. D-APV (50 μM), bicuculline (10 μM) and strychnine (10 μM) were added to the bath solution to isolate AMPA receptor-mediated mEPSCs.

2. Cell-attached and whole-cell recordings and data analysis

Cell-attached capacitance measurements at the release face of the calyx of Held were performed with an SR830 2-phase lock-in amplifier (Stanford Research Systems, Stanford, CA) coupled to an EPC-8 patch-clamp amplifier (HEKA electronics, Lambrecht, Germany)6. A 20 kHz, 200 mV rms sine wave was superimposed on a command potential of 0 mV. The in-phase (real, Re) and 90^{o}-out-of-phase (imaginary, Im) current outputs of the lock-in amplifier were low-pass filtered at 0.3 – 1 ms (24 dB) in most experiments. In experiments requiring higher time resolution, signals were filtered at 0.1 ms, which, together with our sampling rate of 2 – 3.3 kHz, gave a time resolution of ∼0.6 – 0.9 ms (Fig. 1a, right). Methods of cell-attached capacitance recordings, phase adjustment, detection and measurement of capacitance up- and down-steps are described previously6.

The fusion or the fission pore conductance (G_p) was calculated based on

$$G_p=(\Delta Re^2+\Delta Im^2)/\Delta Re \quad (1)$$

where Δ means the difference from baseline31. Based on the G_p value, we estimated the fusion or the fission pore diameter (D_p) based on32

$$D_p=[4\,G_p\rho\lambda/\pi]^{0.5} \quad (2)$$

where ρ is the saline resistivity (100 Ω cm), and #x003BB;, the pore length, is taken as the length of a gap junction channel (15 nm). The fusion G_p usually reached a plateau level in ∼10 ms after fusion, at which we measured the initial G_p value (Fig. 1c). It was followed by a gradual increase for ∼10 – 230 ms before rapid G_p expansion occurred (Fig. 1c).

We estimated that a cell-attached patch at the calyx release face might contain a single to a few active zones6. During application of ∼50 – 100 mM KCl solution, up-steps were observed in 17 out of 55 patches (Fig. 1a, b). The percentage of failure (38/55 or ∼2/3) was similar to that obtained during application of 25 mM KCl in our previous study6. Patch at the residual postsynaptic membrane or the non-release face of the calyx might explain why capacitance up-steps were detected in ∼1/3 of patches6.

Only patches showing up-steps during stimulation were used for data analysis. Up- and down-steps were collected within 500 s after KCl application. In most experiments, we used 50 – 100 mM KCl solution for stimulation. Up- and down- steps, including giant ones, were analyzed from 17 patches showing up- and down-steps during application of ∼50 – 100 mM KCl (Fig. 1b, e, red). Up- and down-steps before KCl application in these 17 patches were not sufficient for plotting their amplitude distribution and cumulative probability curve. To collect more data in control (before KCl application), we included data from additional 61 patches showing up-steps during application of ∼15 – 50 mM KCl solution, which we collected in search of the optimal condition for the generation of giant up-steps. Thus, the control data before KCl application (Fig. 1b, e, black) were collected from 78 patches showing up-steps in response to 15 – 100 mM KCl solution.

Voltage-clamp recordings of EPSC were performed with EPC 10 amplifier33. The series resistance (<10 MΩ) was compensated by 85–95% when the EPSC recording was made.

3. The mEPSC analysis

The mEPSC was analyzed with a mini program (Mini Analysis Program, Synaptosoft Inc., NJ). KCl increased the frequency and the amplitude of mEPSCs. These effects were observed during the first 2 – 3 min of KCl application. We limited data analysis to this period of time for two reasons. First, the frequency of mEPSCs increased to more than 100 Hz as the potassium concentration reached the steady-state. With such a high frequency, the chance for two independent mEPSCs to occur at the same time increased, and the postsynaptic AMPA receptor desensitization might occur, which complicated data analysis. Second, as the potassium concentration approached the steady-state, the membrane resistance of the postsynaptic neuron decreased from 148 ± 9 to 17.5 ± 3 MΩ (n = 5), which was approaching the access resistance (∼7 – 15 MΩ) and thus could decrease the quality of the voltage-clamp. The reason for this decrease is unclear. Both the decrease in the membrane resistance and the change in the reversal potential of potassium channels may contribute to the increase in the inward current during the first 2 min of KCl application (Fig. 3a). Thus, we limited data analysis to within 2 – 3 min after KCl application, during which the membrane resistance was > ∼50 MΩ. Because of a higher noise during KCl application, the threshold of mEPSC detection was set at 20 pA, which also applied to the control condition.

For recordings of mEPSCs during KCl application, we did not compensate the access resistance (<10 MΩ) in most experiments, which reduced the noise. The increase of the mEPSC during KCl application was not due to inadequate voltage-clamp for two reasons. First, the mEPSC amplitude was not increased by KCl application when the extracellular calcium was removed (Fig. 3d). Second, when we compensated the access resistance by 90%, high potassium application still increased the mEPSC amplitude from 31.4 ± 0.9 pA (546 mEPSCs, 4 neurons) in control to 46.2 ± 1.8 pA (2147 mEPSCs, 4 neurons, not shown), similar to those obtained without the access resistance compensation (Fig. 3b).

4. Additional methods

Syt2 knockout mice and electron microscopy are described in Supplementary Information VI.

Supplementary Material

Refer to Web version on PubMed Central for supplementary material.

Acknowledgements

We thank Drs. Jeff Diamond and Ken Paradiso for comments on the manuscript, and Susan Cheng, Rita Azzam and Virginia Crocker for the help in electron microscopy. This work was supported by the National Institute of Neurological Disorders and Stroke Intramural Research Program.

Liming He performed cell-attached recordings. Lei Xue performed EM works, and the mEPSC and EPSC recordings. Jianhua Xu and Benjamin McNeil helped with some experiments. Li Bai helped on EM work and

maintained Syt2$^{-/-}$ mice. Ernestina Melicoff and Roberto Adachi generated the *Syt2*$^{-/-}$ mouse line. Ling-Gang Wu supervised the project and wrote the paper.

Reference List

1. Sudhof TC. The synaptic vesicle cycle. Annu. Rev. Neurosci. 2004; 27:509–547. [PubMed: 15217342]
2. Alvarez, dT; Fernandez, JM. Compound versus multigranular exocytosis in peritoneal mast cells. J Gen. Physiol. 1990; 95:397–409. [PubMed: 2324701]
3. Scepek S, Lindau M. Focal exocytosis by eosinophils–compound exocytosis and cumulative fusion. EMBO J. 1993; 12:1811–1817. [PubMed: 8491174]
4. Heidelberger R, Heinemann C, Neher E, Matthews G. Calcium dependence of the rate of exocytosis in a synaptic terminal. Nature. 1994; 371:513–515. [PubMed: 7935764]
5. Matthews G, Sterling P. Evidence that vesicles undergo compound fusion on the synaptic ribbon. J. Neurosci. 2008; 28:5403–5411. [PubMed: 18495874]
6. He L, Wu XS, Mohan R, Wu LG. Two modes of fusion pore opening revealed by cell-attached recordings at a synapse. Nature. 2006; 444:102–105. [PubMed: 17065984]
7. Sätzler K, et al. Three-dimensional reconstruction of a calyx of Held and its postsynaptic principal neuron in the medial nucleus of the trapezoid body. J Neurosci. 2002; 22:10567–10579. [PubMed: 12486149]
8. Gentet LJ, Stuart GJ, Clements JD. Direct measurement of specific membrane capacitance in neurons. Biophys. J. 2000; 79:314–320. [PubMed: 10866957]
9. Heuser JE, Reese TS. Evidence for recycling of synaptic vesicle membrane during transmitter release at the frog neuromuscular junction. J. Cell Biol. 1973; 57:315–344. [PubMed: 4348786]
10. de Lange RP, de Roos AD, Borst JG. Two modes of vesicle recycling in the rat calyx of Held. J. Neurosci. 2003; 23:10164–10173. [PubMed: 14602833]
11. Richards DA, Guatimosim C, Betz WJ. Two endocytic recycling routes selectively fill two vesicle pools in frog motor nerve terminals. Neuron. 2000; 27:551–559. [PubMed: 11055437]
12. Coggins MR, Grabner CP, Almers W, Zenisek D. Stimulated exocytosis of endosomes in goldfish retinal bipolar neurons. J. Physiol. 2007; 584:853–865. [PubMed: 17823206]
13. Xu J, et al. GTP-independent rapid and slow endocytosis at a central synapse. Nat. Neurosci. 2008; 11:45–53. [PubMed: 18066059]
14. Sun J, et al. A dual-Ca2+-sensor model for neurotransmitter release in a central synapse, Nature. Nature. 2007; 450:676–682. [PubMed: 18046404]
15. Korogod N, Lou X, Schneggenburger R. Presynaptic Ca2+ requirements and developmental regulation of posttetanic potentiation at the calyx of Held. J Neurosci. 2005; 25:5127–5137. [PubMed: 15917453]
16. Habets RL, Borst JG. Post-tetanic potentiation in the rat calyx of Held synapse. J Physiol. 2005; 564:173–187. [PubMed: 15695246]
17. Zucker RS, Regehr WG. Short-term synaptic plasticity. Annu. Rev. Physiol. 2002; 64:355–405. [PubMed: 11826273]
18. Heuser JE. Proceedings: A possible origin of the 'giant' spontaneous potentials that occur after prolonged transmitter release at frog neuromuscular junctions. J Physiol. 1974; 239:106P–108P.
19. Henze DA, McMahon DB, Harris KM, Barrionuevo G. Giant miniature EPSCs at the hippocampal mossy fiber to CA3 pyramidal cell synapse are monoquantal. J Neurophysiol. 2002; 87:15–29. [PubMed: 11784726]
20. Llano I, et al. Presynaptic calcium stores underlie large-amplitude miniature IPSCs and spontaneous calcium transients. Nat. Neurosci. 2000; 3:1256–1265. [PubMed: 11100146]
21. Wall MJ, Usowicz MM. Development of the quantal properties of evoked and spontaneous synaptic currents at a brain synapse. Nat. Neurosci. 1998; 1:675–682. [PubMed: 10196583]
22. Del Castillo J, Katz B. Quantal components of the end-plate potential. J. Physiol. 1954; 124:560–573. [PubMed: 13175199]

23. Tong G, Jahr CE. Multivesicular release from excitatory synapses of cultured hippocampal neurons. Neuron. 1994; 12:51–59. [PubMed: 7507341]
24. Wadiche JI, Jahr CE. Multivesicular release at climbing fiber-Purkinje cell synapses. Neuron. 2001; 32:301–313. [PubMed: 11683999]
25. Sun JY, Wu LG. Fast kinetics of exocytosis revealed by simultaneous measurements of presynaptic capacitance and postsynatpic currents at a central synapse. Neuron. 2001; 30:171–182. [PubMed: 11343653]
26. Singer JH, Lassova L, Vardi N, Diamond JS. Coordinated multivesicular release at a mammalian ribbon synapse. Nat. Neurosci. 2004; 7:826–833. [PubMed: 15235608]
27. Paillart C, Li J, Matthews G, Sterling P. Endocytosis and vesicle recycling at a ribbon synapse. J Neurosci. 2003; 23:4092–4099. [PubMed: 12764096]
28. Oertel D. The role of timing in the brain stem auditory nuclei of vertebrates. Annu. Rev. Physiol. 1999; 61:497–519. [PubMed: 10099699]
29. Boraud T, Bezard E, Bioulac B, Gross CE. From single extracellular unit recording in experimental and human Parkinsonism to the development of a functional concept of the role played by the basal ganglia in motor control. Prog. Neurobiol. 2002; 66:265–283. [PubMed: 11960681]
30. Takamori S, et al. Molecular anatomy of a trafficking organelle. Cell. 2006; 127:831–846. [PubMed: 17110340]
31. Lindau M, Alvarez de Toledo G. The fusion pore. Biochim. Biophys. Acta. 2003; 164:167–173. [PubMed: 12914957]
32. Spruce AE, Breckenridge LJ, Lee AK, Almers W. Properties of the fusion pore that forms during exocytosis of a mast cell secretory vesicle. Neuron. 1990; 4:643–654. [PubMed: 2344404]
33. Xu J, Wu LG. The decrease in the presynaptic calcium current is a major cause of short-term depression at a calyx-type synapse. Neuron. 2005; 46:633–645. [PubMed: 15944131]

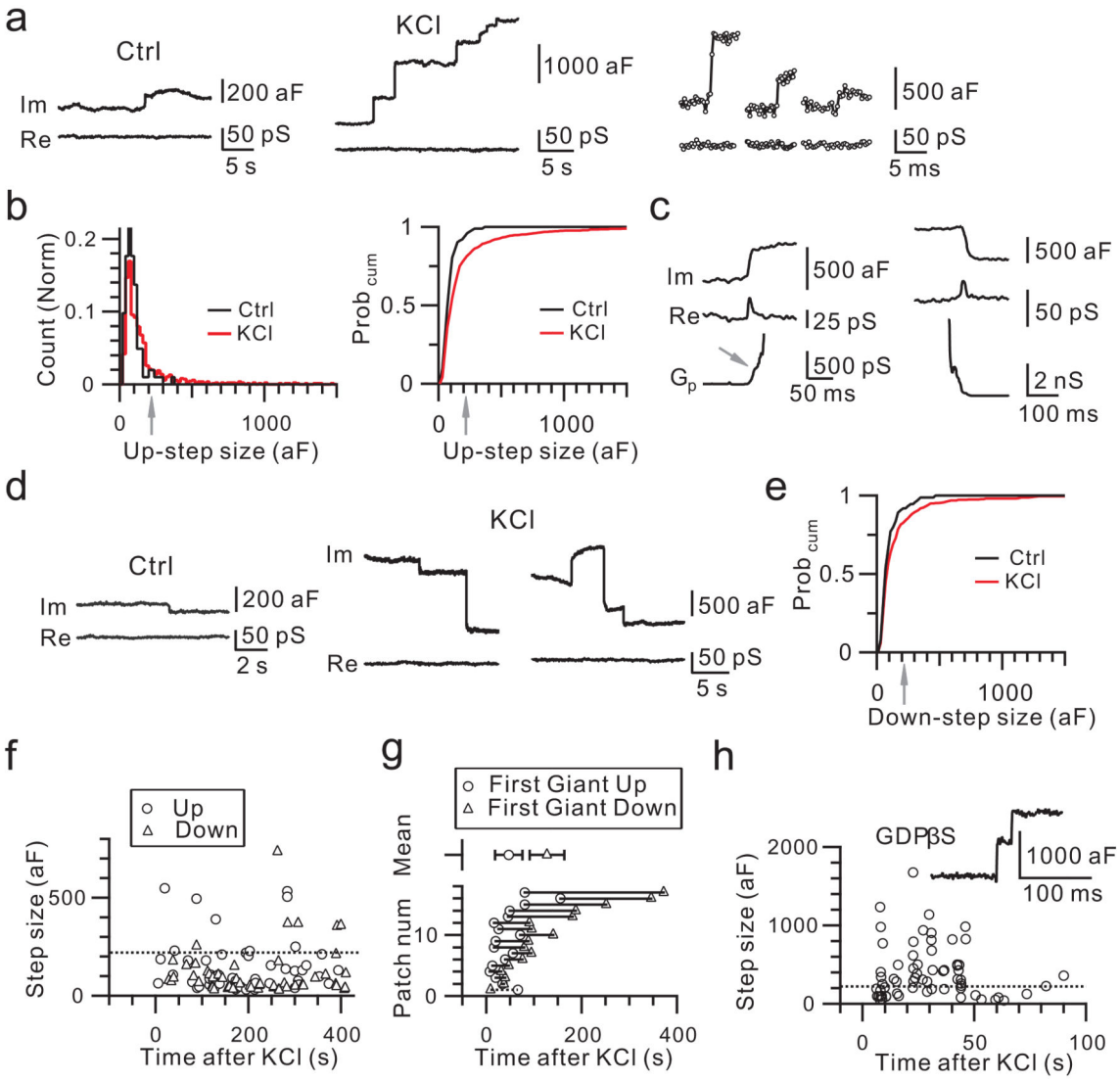

Figure 1. Giant capacitance up- and down-steps

a, Sampled imaginary (Im, capacitance) and real (Re, conductance) components of the complex admittance in control (left) and in KCl solution (middle, right). Right: sampling interval was 0.3 ms.

b, The up-step amplitude distribution and cumulative probability curve ($Prob_{cum}$) in control (102 up-steps, 78 patches) and in KCl (857 up-steps, 17 patches). Arrows indicate 220 aF. **c**, G_p during a giant up- (left) and down-step (right) in KCl. Arrow indicates initial G_p.

d, Down-steps in control (left) and in KCl (middle, right).

e, The down-step amplitude $Prob_{cum}$ in control (74 down-steps, 78 patches) and in KCl (591 down-steps, 17 patches).

f, Up- and down-steps induced by KCl from a patch. Dotted line indicates 220 aF.

g, The timing of the first giant up- and down-step for each of 17 patches and their mean (± s.e.m, upper, $p < 0.01$).

h, Similar to f, but with GDPβS (0.3 mM) dialyzed into the calyx via a whole-cell pipette. Insert: sampled up-steps.

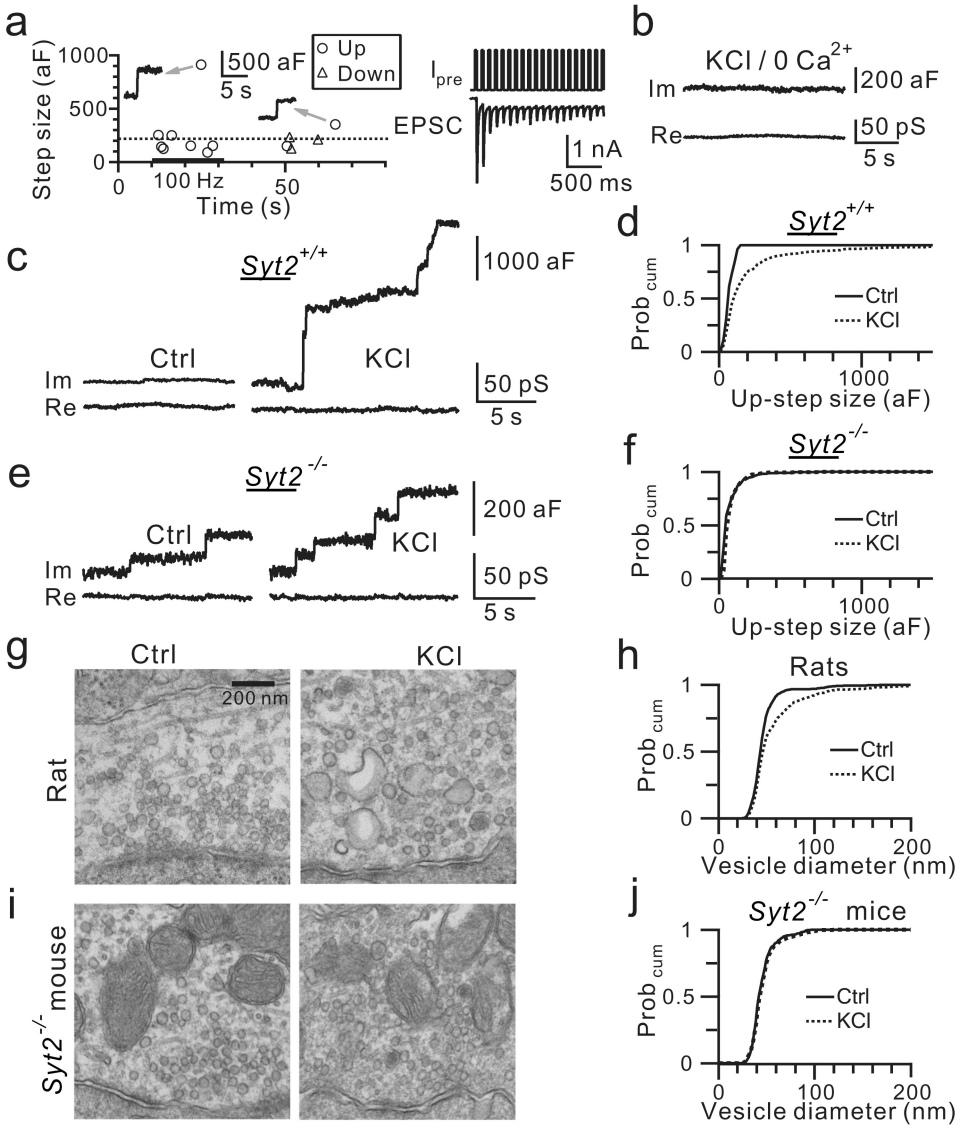

Figure 2. Calcium/Syt2 mediates compound fusion

a, Left: Up-steps were induced by current injection (1 nA, 3 ms, 100 Hz, 20 s, bar) via another cell-attached patch at the same calyx. Dotted line indicates 220 aF. Arrows indicate sampled up-steps. Right: Calyx cell-attached current injection (I_{pre}) induced calyx action potentials and thus EPSCs from a synapse without postsynaptic neuron removal14.

b, Im and Re in KCl with no extracellular calcium.

c, Up-steps in control and in KCl from a *Syt2*$^{+/+}$ mouse.

d, The up-step amplitude $Prob_{cum}$ in control (26 up-steps, 11 patches) and in KCl (483 up-steps, 11 patches) from 8 *Syt2*$^{+/+}$ mice.

e–f, Similar to c–d, but from 9 *Syt2*$^{-/-}$ mice (control: 220 up-steps, 10 patches; KCl: 812 up-steps, 10 patches).

g, EM images of rat calyx in control and in KCl.

h, The vesicle diameter $Prob_{cum}$ in control (2896 vesicles) and in KCl (2040 vesicles) from 6 rats.

i–j, Similar to g–h, but from 4 *Syt2*$^{-/-}$ mice (Control: 1298 vesicles; KCl: 1053 vesicles).

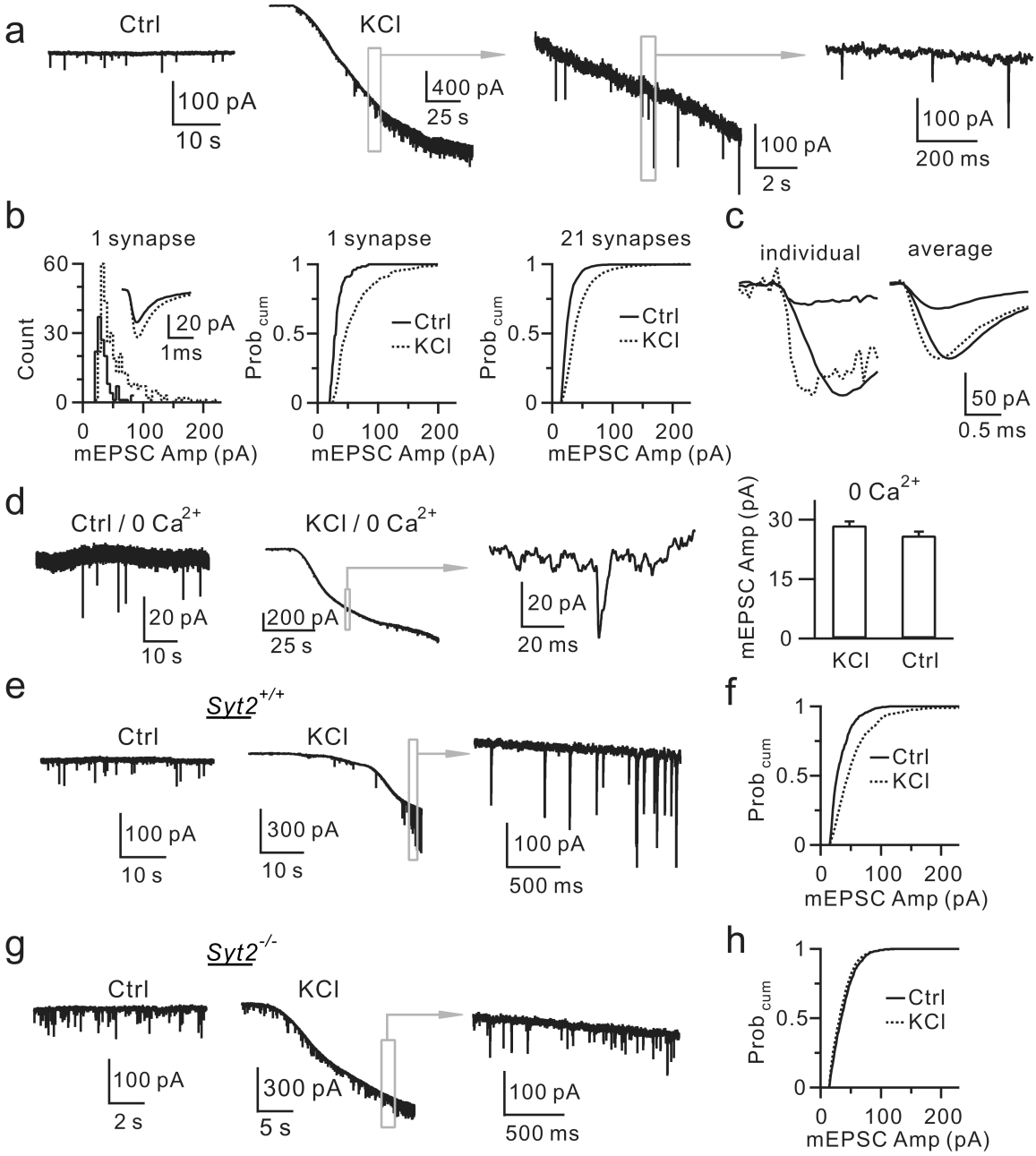

Figure 3. KCl induces calcium/Syt2-dependent increase of the mEPSC size

a, mEPSCs in control and in KCl (traces in boxes are enlarged).

b, The distribution and the $Prob_{cum}$ for the mEPSC amplitude in control and in KCl from 1 (inset shows the mean) and 21 synapses (control: 4302 mEPSCs; KCl: 16006 mEPSCs).

c, Left: a small and a large mEPSC (solid), and the scaled small mEPSC (dotted). Right: the mean of mEPSCs < 80 pA and ≥ 80 pA (solid), and the scaled small mEPSC (dotted) from 1 synapse.

d, Sampled mEPSCs and the mEPSC amplitude (± s.e.m., 5 neurons) in control and in KCl with 0 extracellular calcium. Right: 270 mEPSCs in control; 324 mEPSCs in KCl ($p > 0.3$).

e, mEPSCs in control and in KCl from a *Syt2*$^{+/+}$ mouse.

f, The mEPSC amplitude $Prob_{cum}$ in control (1788 mEPSCs, 6 synapses) and in KCl (3360 mEPSCs, 6 synapses) from 4 *Syt2*$^{+/+}$ mice.

g–h, Similar to e-f, but from 6 *Syt2*$^{-/-}$ mice (Ctrl: 3780 mEPSCs, 9 synapses; KCl: 8224 mEPSCs, 9 synapses).

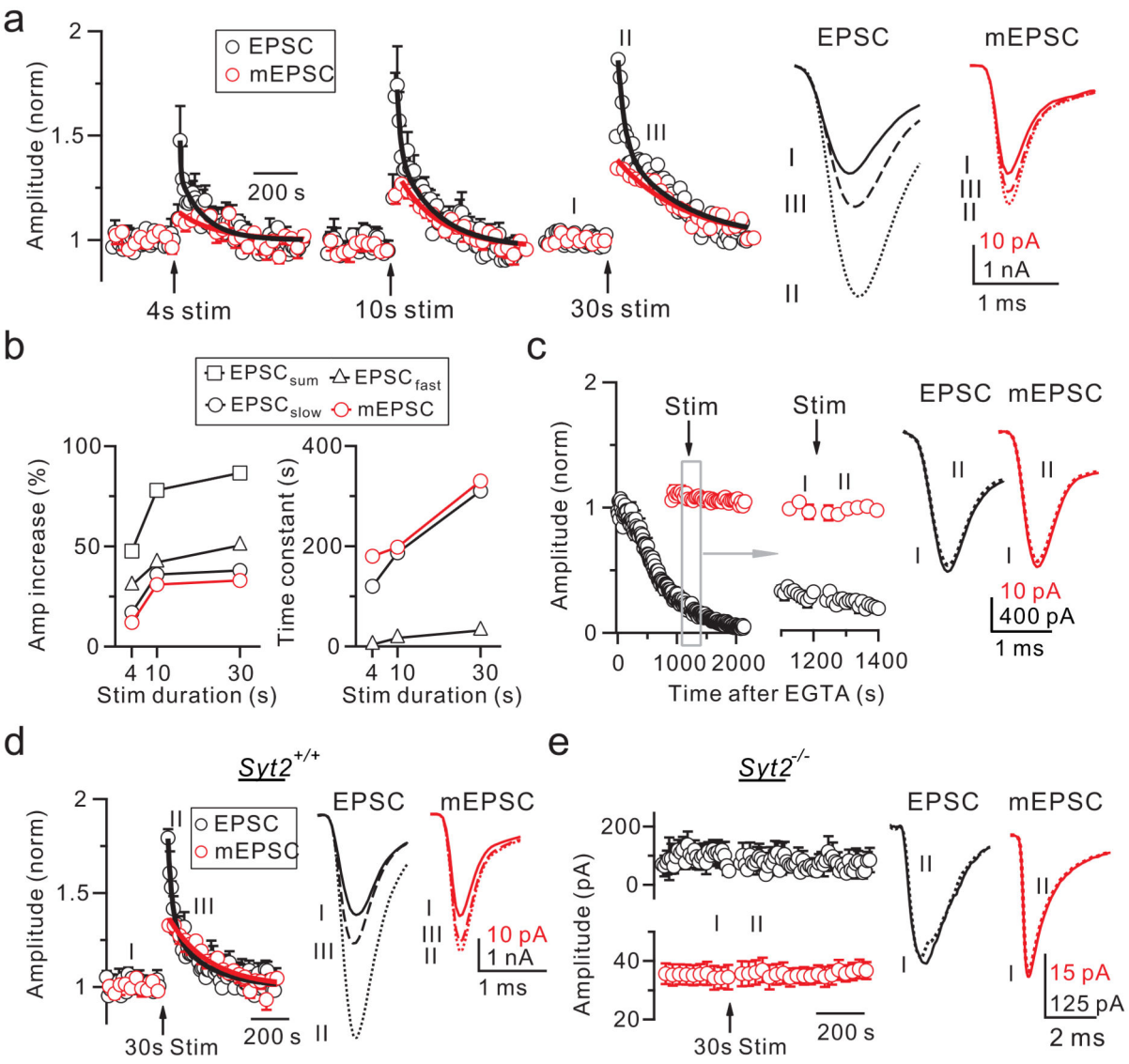

Figure 4. Calcium/Syt2-dependent PTP and quantal size increase

a, EPSC and mEPSC amplitude change (normalized) induced by a 100 Hz train (arrows) for 4, 10, and 30 s (± s.e.m, 5 – 7 synapses). The EPSC potentiation was fitted bi-exponentially (black curve), whereas the mEPSC, fitted mono-exponentially (red curve). Sampled EPSCs and mEPSCs taken at times labeled, are shown (right).

b, The amplitude and the time constant of the bi- or mono-exponential fit obtained in panel a are plotted. The bi-exponential fit includes fast ($EPSC_{fast}$) and slow ($EPSC_{slow}$) component and their sum ($EPSC_{sum}$).

c–e, Similar to panel a (30 s train only), but with EGTA-AM in bath solution (c: 200 μM, applied at time 0), or in *Syt2*$^{+/+}$ (d, 7 synapses, 5 mice) or *Syt2*$^{-/-}$ mice (e, 7 synapses, 6 mice). d: the EPSC increase was fitted bi-exponentially (τ_1 = 25 s, 46%; τ_2 = 199 s, 33%), whereas the mEPSC increase, fitted mono-exponentially (τ = 226 s, 37%).